

Assessing Leak Paths in the Cement Sheath of a Cased Borehole by Analysis of Monopole Wavefield Modes

Hua Wang^{1,2,*}, Michael Fehler² and Aimé Fournier²

¹ *University of Electronic Science and Technology of China, Chengdu, Sichuan, 611731, P.R. China.*

² *Earth Resources Laboratory, Massachusetts Institute of Technology, Cambridge, MA, 02139, USA.*

Received 4 May 2018; Accepted (in revised version) 3 December 2018

Abstract. Evaluation of possible leakage pathways of CO₂ injected into geological formations for storage is essential for successful Carbon Capture and Storage (CCS). A channel in the borehole cement, which secures the borehole casing to the formation, may allow CO₂ to escape. Risk assessment and remediation decisions about the presence of such channels depend on channel parameters: radial position r from the center of the borehole; channel thickness d ; azimuthal position φ of the channel; and azimuthal extent θ of the channel. Current state-of-the-art cement-bond logging technology, which uses only the first arrival at a centralized borehole receiver, can diagnose limited details about CO₂ leak channels. To accurately characterize the possible leak paths in the cement, we use a 3-dimensional finite-difference method to investigate the use of the abundant data collected by a modernized monopole sonic tool that contains an array of azimuthally distributed receivers. We also investigate how to improve the tool design to acquire even more useful information. For cases where borehole fluid is either water or supercritical CO₂, we investigate various receiver geometries, multimodal analyses of multi-frequency data to discover the type of logging tool that provides the best information for CCS management. We find that an appropriate choice of wave modes, source frequencies, source polarities, and receiver locations and offsets provides sensitivity to d , φ , θ . The amplitude of the first arrival from a monopole source is sensitive to θ . Amplitudes at receivers at different azimuths are sensitive to φ . The slow Stoneley mode (ST2) velocity is sensitive to d , but ST2 is not easy to pick when θ and d are small. Further improvement is necessary to provide comprehensive information about possible flow channels in casing cement.

AMS subject classifications: 86A15

Key words: Greenhouse effect, CO₂ leak channel, cement bond evaluation, borehole acoustic logging, casing wave, Stoneley waves.

*Corresponding author. *Email addresses:* huawang@uestc.edu.cn (H. Wang), fehler@mit.edu (M. Fehler), aime@mit.edu (A. Fournier)

1 Introduction

Carbon capture and storage (CCS) is essential to mitigating the “greenhouse” effect and ocean acidification. Geological storage involves injecting large amounts of CO₂ into underground formations, followed by measurement, monitoring, and verification of the surrounding site to ensure that no CO₂ leaks out [1, 2]. Evaluation of possible leakage pathways is essential [3], as it also is for plug-and-abandon activities in petroleum wells [4–7].

Fig. 1 shows some of the many possible leakage pathways that may occur in or near to a wellbore [8], many of which may not be detected using conventional well-log analysis. The leak paths labeled b and c in the cement plug cannot be evaluated by well logs. Other leak paths may be detected by well logs [9, 10]. Boreholes are cased with steel that is cemented into place, so micro-debonding at the casing steel interface and fractures in cement are significant issues. In addition, possible leaks at the cement-casing (leak path a in Fig. 1) and cement-formation (leak path f in Fig. 1) interfaces (called I and II here) need to be distinguished. Detection of leaks in boreholes with multiple casing strings (one inside another) present even more challenges [4–7].

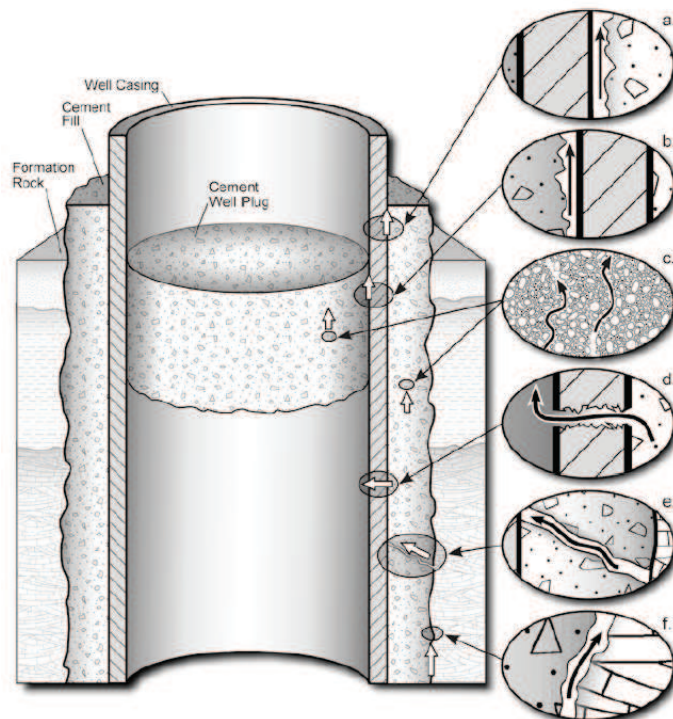


Figure 1: Possible leakage pathways: a) between casing and cement; b) between cement plug and casing; c) through pore space in cement resulting from cement degradation; d) through casing corrosion; e) through cement fractures; f) between cement and rock. From Figure 1 in [8].

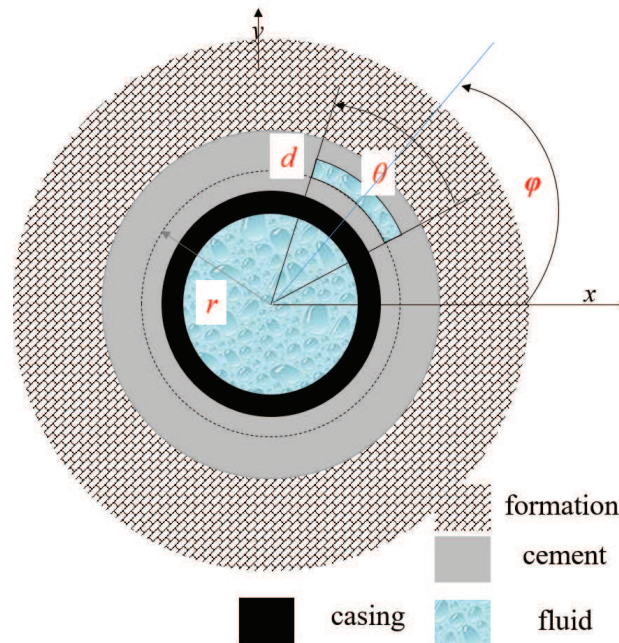


Figure 2: Horizontal section through borehole model showing positions of fluid, casing, cement and formation. The 4 parameters that we use to describe a fluid channel in the cement are illustrated.

A cylindrical fluid channel in the annulus between casing and formation, which may allow CO_2 leakage, may be described by 4 parameters [11]. Two describe the location of the channel: radial position r of the channel; and azimuthal position φ . The dimensions of the channel are described by its thickness d and its angular extent θ (Fig. 2).

Acoustic wireline logging methods, including those using sonic (i.e., tens of kHz) frequencies [4, 12–15] and ultrasonic (above 100 kHz) frequencies [16–18] have been used to evaluate the quality of cement and the bonds between the casing and formation. These two methods are usually combined to obtain a more comprehensive evaluation of the cement and the bonds, especially when evaluating for gas invasion [19].

The state-of-the-art sonic methods CBL (cement bond logging) and VDL (variable density logging) only work if the channel is at Interface I ($r = \text{casing outer radius}$), and can estimate only one parameter that is some combination of d and θ , and then has no resolution of φ [12, 13, 20]. Recent studies show that φ can be estimated from the distribution of measured sector amplitude by a newly designed segmental CBL tool [21] or the conventional segmented bond tool [22]. These studies only considered the case where d equals the annulus thickness. Wang and Fehler [23] found that the velocity of a slow Stoneley wave, appearing when the cement is partially replaced by fluid for the case where $\theta = 360^\circ$, is only sensitive to the total thickness of the fluid channel.

Although the newly developed ultrasonic pitch-catch method [6, 17, 18] combined with the pulse-echo method shows promise for evaluating the bonding condition at in-

terface II, it is still challenged by eccentricity of the casing i.e., casing center not at the borehole center and roughness of the interface [5,24].

With the development of new logging tools [25], we may have the capability to obtain and analyze full-waveform recordings at different azimuths and source-receiver offsets. It is thus useful to develop new methods to analyze borehole logging data and to improve the ability to evaluate cement integrity. Quantification of the sensitivity of the measurements to source frequency and receiver positioning (azimuths and offsets) may also inform new logging tool designs for evaluating cement.

2 Full-waveform method

We calculate acoustic waves using a 3DFD (3 Dimensional Finite-Difference) code [6,26], which has been validated for cased hole models by Wang and Fehler [23]. The cased-hole model consists of multiple concentric cylinders and a fluid channel variably positioned in the annulus between casing and formation, as shown in Fig. 2. An industry-standard 9 5/8 inch (about 24.45 cm) casing is used. The casing thickness is 14 mm. Table 1 lists the geometries and elastic parameters of our example fully cemented cased-hole model. The fluid in the channel is taken to be the same as the borehole fluid.

Table 1: Elastic parameters for the model used in our study.

Medium	V_p (m/s)	V_s (m/s)	Density (kg/m ³)	Radius (mm)
Fluid	1500	0	1000	108
Steel	5500	3170	8300	122
Cement	3000	1730	1800	170
Sandstone	4500	2650	2300	300 to 424.2

We vary the 4 parameters shown in Fig. 2 that describe the fluid channel, to investigate the sensitivity of different borehole modes to differing bonding conditions. A Ricker wavelet having various central frequencies is used as the source function. The simulation model size is 0.6 m (x) by 0.6 m (y) by 4.55 m (z). Non-reflective boundary conditions are placed at the model boundaries [27]. Grid sizes of 2 mm in x and y , and 4 mm in z directions are used in the 3DFD code.

First, we investigate the wave propagation by examining wavefield snapshots for four different models. Model (1) is used to simulate a good cement case ($r = 122\text{mm}$, $d = 0\text{mm}$, $\theta = 0^\circ$, and $\varphi = 0^\circ$). Model (2) is used to simulate an extreme case of leak path e in Fig. 1 and model (3) is for leak path a. Four parameters in model (2) are: $r = 122\text{mm}$, $d = 48\text{mm}$, $\theta = 360^\circ$, and $\varphi = 0^\circ$ and in model (3) are: $r = 122\text{mm}$, $d = 8\text{mm}$, $\theta = 90^\circ$, and $\varphi = 0^\circ$. For Model (4), we replace the fluid in the channel in model (3) with supercritical CO₂. The compressional velocity and density of CO₂ are chosen as 500m/s and 800kg/m³ [28]. In these initial calculations, the effect of the tool is ignored and a centralized point source with a 10kHz Ricker wavelet is used. Fig. 3 shows vertical section wavefield snapshots

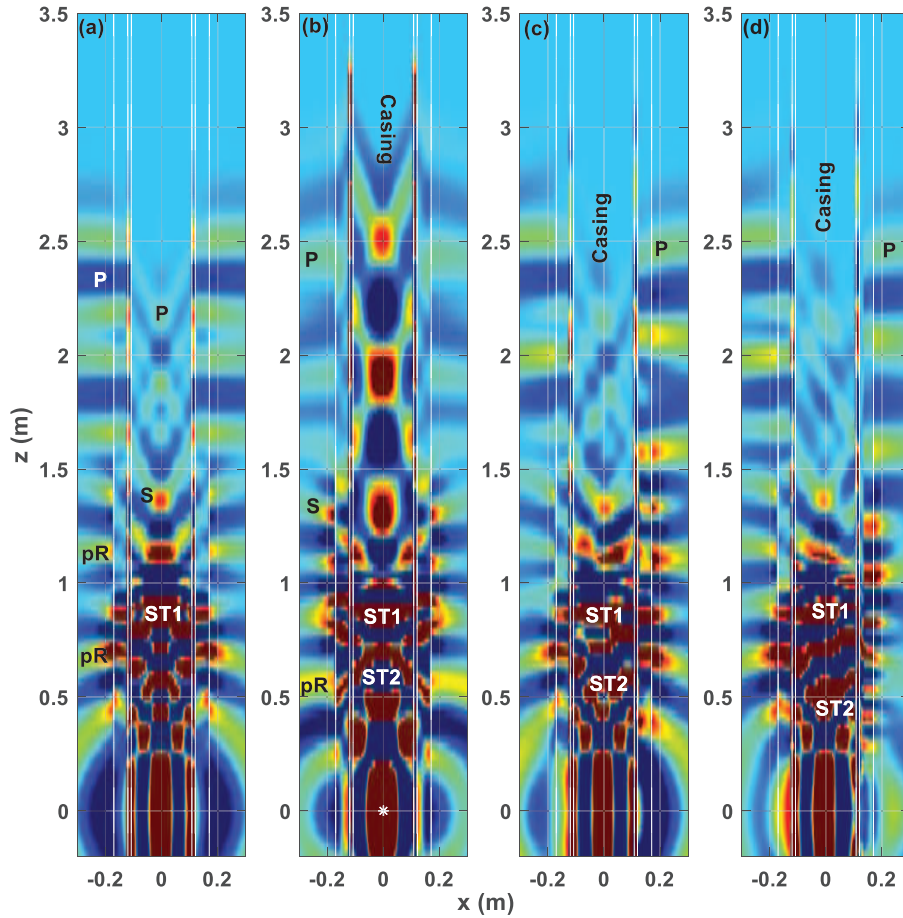


Figure 3: Vertical section through 60–cm wide borehole model (including formation) with a 10–kHz monopole source centered at $z=0$, showing acoustic waves at $t=0.8\text{ms}$ for (a) good cement ($r=122\text{mm}$, $d=0$, $\theta=0^\circ$, and $\varphi=0^\circ$), (b) no cement ($r=122\text{mm}$, $d=48\text{mm}$, $\theta=360^\circ$, and $\varphi=0^\circ$), (c) cement containing a partial fluid channel ($r=122\text{mm}$, $d=8\text{mm}$, $\theta=90^\circ$, and $\varphi=0^\circ$), and (d) same geometry as (c) except for the channel filled with a super-critical CO_2 . The two innermost lines around $x=0$ are the inner boundaries of the casing, the two outermost lines are boundaries between the borehole wall and the formation, and the other two lines are the outer boundary of the casing. Source position is marked by a white star in (b).

at 0.8ms for four models: (a) good cement, (b) no cement, (c) cement containing a partial fluid channel, and (d) cement containing a partial CO_2 channel. The source location is marked by a white star in Fig. 3b. The two innermost lines around $x=0$ are the inner boundaries of the casing and the two outermost lines are the boundaries of the borehole wall, and the other two lines are the outer boundary of the casing. The good-cement and no-cement cases were previously investigated by Wang and Fehler [23, 29]. From their description, we know that there are casing, P, S, pR (pseudo-Rayleigh), and Stoneley (ST) waves in the cased-hole models. These modes are marked in Figs. 3a and 3b. The casing modes are trapped in the casing and do not leak into the borehole when the cement

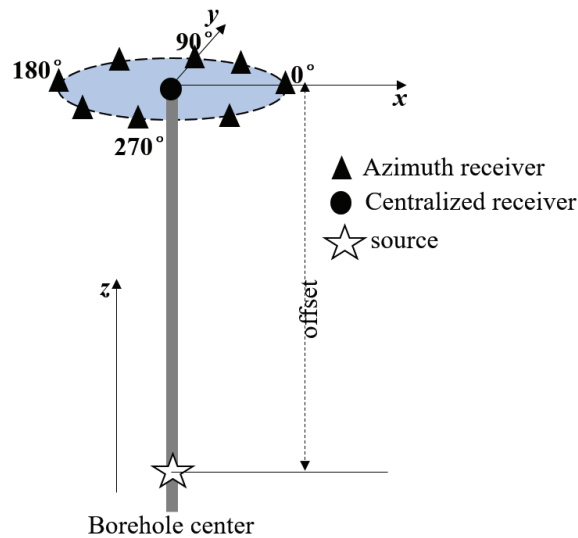


Figure 4: Schematic diagram for source and receiver configuration. Radius of the circle containing the azimuthally distributed receivers is 46mm.

between the casing and formation is good, as shown in Fig. 3a. Formation P and S waves can be observed in the fluid inside the casing. However, when there is no cement, in Fig. 3b, the casing modes leak into the fluid columns both inside and outside of the casing. Then the first arrival in the borehole fluid is a casing mode. A slow Stoneley mode, marked ST2 in Fig. 3b, appears when cement is replaced by fluid. For the partial fluid channel in Fig. 3c, the wavefield is a mixture of the wavefields seen in Figs. 3a and 3b. The first arrival is a casing mode and this is not visible because of its small amplitude. There is also ST2 in the wavefield. The symmetry of the wavefield is broken because the model is non-axisymmetric. This indicates the possibility of identification of the azimuth of the channel by using the azimuthal variation of the waveforms. When the channel is filled by a super-critical CO_2 (Fig. 3d), the non-axisymmetric wavefield is obvious and possibly stronger than when water is present (see e.g., $z > 1.5\text{m}$) and the ST2 wave is slower than in Fig. 3c because of the slower velocity of CO_2 .

We now investigate waveforms collected by 8 azimuthally distributed receivers and one centralized receiver at different offsets, as shown in Fig. 4. The radius of the azimuthally distributed receiver array is 46mm, which is the radius of the most common downhole sonic tool. Fig. 5 shows the waveforms at a 3-m offset centralized receiver for different models. Fig. 5a shows the full waveform and Fig. 5b shows the magnified first arrival. The first arrival in the good cement case is the formation P wave (lower trace in Fig. 5a). The following waves are clear S, pR, ST1, and pR Airy waves, as marked in Fig. 5a. When the cement is not well bonded along all or a portion of the interface between cement and casing (upper two traces in Fig. 5a), the formation P wave is no longer the first arrival and is concealed within the casing waves. In these cases, the S arrival

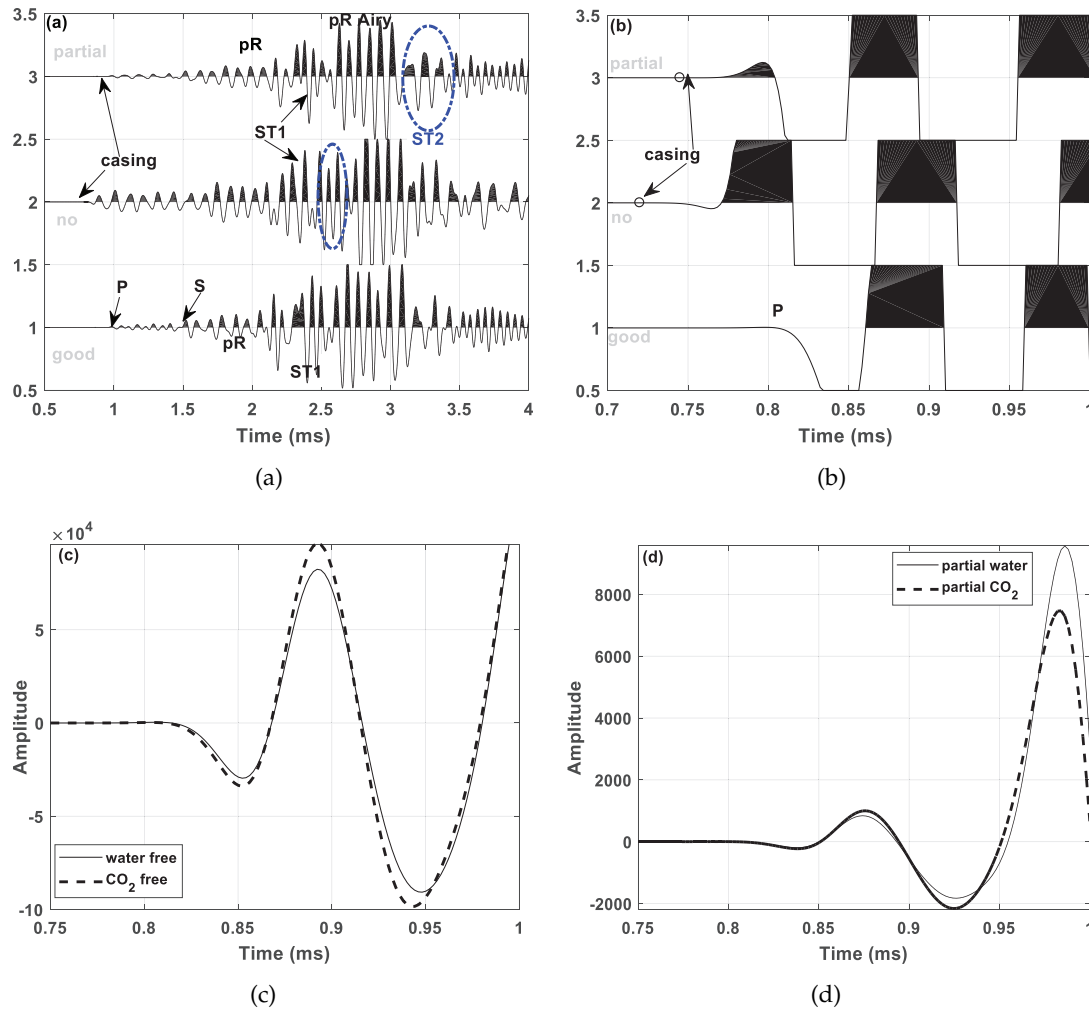


Figure 5: Waveforms at a 3m offset centralized receiver for different models. (a) Full waveform. (b) Magnified first arrivals. Comparison of first arrivals between water and CO_2 cases: no cement (c) and partial channel (d). Different modes are marked. Nomenclature: good means good cement between casing and borehole, no means no cement, partial means a fluid layer that covers an azimuth of 90° exists at the casing-cement boundary. Arrival time of first arrivals of no cement and partial channel cases are marked with circles.

is not easily identified. In addition to ST1 in the borehole fluid, a slow ST wave (ST2 as marked by a blue dashed circle on the top trace of Fig. 5a) appears that is related to the fluid channel between the casing and cement. The first-arrival time in the partial cement case is between the casing arrival seen in the no-cement case and formation P arrival. The presence of this arrival could be misinterpreted as indicating good cement at interface I but bad cement at interface II (see Fig. 12c in [23]). If the fluid is replaced with the super-critical CO_2 , the amplitude of the first arrival is larger than when the fluid is water (Figs. 5c and 5d). However, the fluid type does not change the first arrival time.

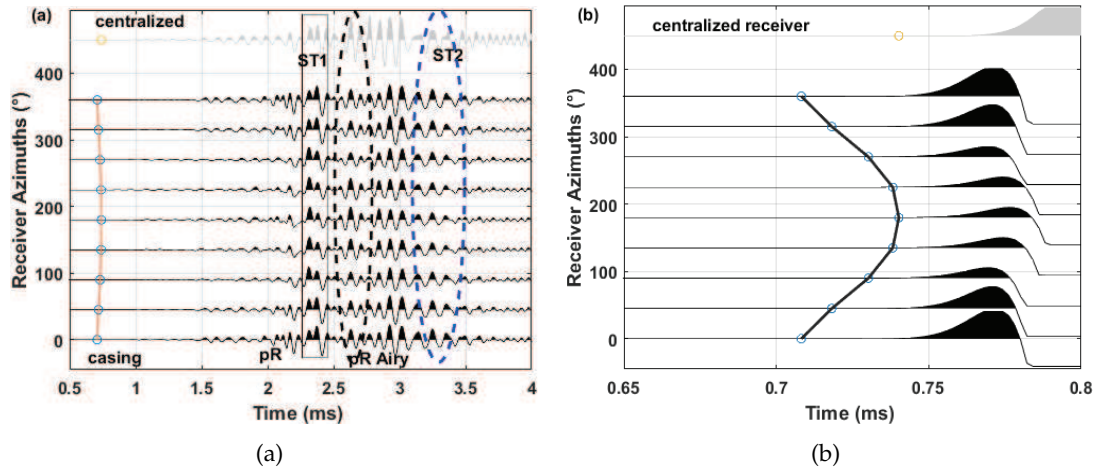


Figure 6: Waveforms at azimuthally distributed receivers for model 3: partial water channel ($r = 122\text{mm}$, $d = 8\text{mm}$, $\theta = 90^\circ$, and $\varphi = 0^\circ$). (a) Full waveform. (b) Magnified first arrivals. Gray curves are the waveform at the centralized receiver. The offset is 3m.

Figs. 6a and 6b show the full waveforms and magnified first arrivals on the azimuthally distributed receivers at 3–m offset for the partial channel model with water. The waveform obtained at the centralized receiver is also shown (gray curves). The first-arrival times picked on greatly amplified traces are plotted using a solid black curve with circles in Fig. 6b. They exhibit a U-shaped curve with azimuth angle, where the maximum is at the receiver at 180° and minimum is at the receiver at 0° or 360° . The minimum arrival time is the same as the arrival time of centralized wave in the no-cement case. If the first-arrival time at the centralized receiver is used and the first-arrival times on the azimuthally distributed waveforms are not used, the bond condition would be misinterpreted as good cement at interface I but bad cement at interface II, see Fig. 12c in [23]. Here we find that using the first arrivals at the azimuthally distributed receiver array allows one to avoid the misinterpretation obtained by using the first-arrival time at the centralized receiver for case of $0^\circ < \theta < 360^\circ$.

In addition to arrival-time differences, the amplitude of the peak of the first arrivals also varies with azimuth angle of the receivers. The maximum first-arrival amplitude is at 0° , which is the azimuth φ of the fluid channel. The minimum is at 180° , the furthest location from the fluid channel. Both arrival times and amplitudes of the first arrivals at the azimuthally distributed receivers can be used to determine φ of the fluid channel. Amplitudes of pR and ST1 waves also change with receiver azimuth when there is a partial fluid channel. To investigate the azimuthal variation of other phases, Fig. 7 shows the amplitudes of the first peak, ST1, and a pR (marked with a black ellipse in Fig. 6) with receiver azimuth. The first-arrival times are also shown. All the parameters are normalized by their maximum. The radial direction is the magnitude of the parameter and the azimuth is the receiver azimuth angle (see Fig. 4). Although we can determine

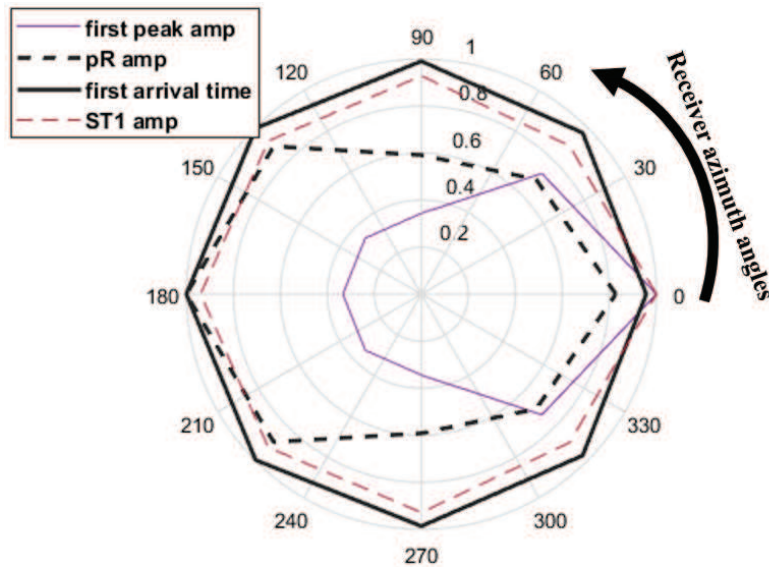


Figure 7: Azimuthal variation of waveform characteristics in model containing a water channel. All the parameters are normalized by their maximum. The radial direction is the magnitude of the parameter and the azimuth is that of the receiver relative to the center of the fluid channel (see Fig. 4).

φ from the azimuth having minimum amplitude of ST1 and the minimum first-arrival time, the small azimuthal variations make them difficult to use. The amplitude of the selected pR Airy phase is much more sensitive to φ than the ST1 amplitude and the arrival time. However, the character of the pR Airy changes with formation velocities and is not easy to pick in some formations. The amplitudes of other pR phases are also not easy to pick due to their strong dispersion. The ST2 wave amplitude, which is not shown in Fig. 7 is not easy to pick because it is hard to pick the same phase at different receiver azimuths. A realistic way is to obtain the ST2 velocity using a semblance method [30] that provides the dispersion characteristics of ST2 and allows us to determine where in the waveform to pick ST2. The first-arrival amplitude is the most sensitive one among the four parameters. We can determine φ from the maximum first-arrival amplitude. In the experiment section, we focus on the first-arrival amplitude and the ST2 wave velocity for different cases.

3 Experiments and results

Full-waveform simulation enables the new borehole evaluation method to estimate the parameters shown in Fig. 2 that describe a fluid channel. To assess the sensitivities of source-receiver design to the parameters, a total of 1323 (r , d , θ , φ) combinations were simulated: 7 values of φ (0, 15, 30, 45, 60, 75, and 90°), 7 of θ (30, 90, 150, 210, 270, 330, and 360°), 3 of d (8, 16, and 48mm), and 9 source frequencies (4, 6, 8, 10, 12, 14, 16, 18, and

20kHz). r was fixed at 122mm. This value of r means that the channel is at the casing-cement interface. Thus, our simulations can be considered as appropriate for assessing debonding at the casing-cement interface.

3.1 ST2 velocity

Since the arrival time of ST2 does not change with receiver position (azimuth or centralized), as shown in Fig. 6a, we use the array waveforms along a centralized receiver array to calculate the ST2 velocity by a semblance method [30]. Fig. 8 shows the extracted velocity-frequency dispersion characteristics of the ST1 and ST2 waves from the array waveforms. We used centralized receiver-array offsets ranging from 3.00 to 3.98m with 0.14m interval between the 8 receivers. Figs. 8a and 8b show the results for two values of θ , 150 and 360°, where the fluid-channel parameters are $d = 16\text{mm}$, $\varphi = 0^\circ$, $r = 122\text{mm}$. The modal dispersion curve for ST2, when $\theta = 360^\circ$, is shown using a dashed line [23]. We find that although the coherence of ST2 becomes weak when θ is smaller, the velocity of ST2 remains roughly the same for different values of θ . We show two examples in Figs. 8c and 8d, where $d = 48\text{mm}$. The solid curves are the modal dispersion of the

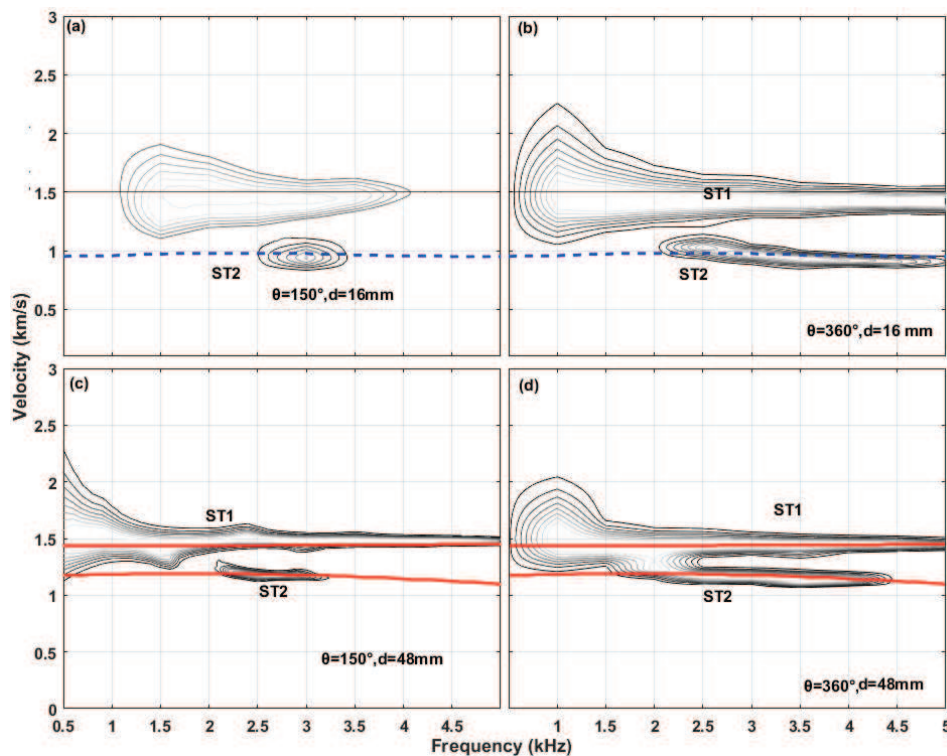


Figure 8: Dispersion analysis for the waveforms at centralized receiver array consisting of 8 receivers having offsets from 3 to 3.98m with 0.14m interval. Fluid channel parameters are $r = 122\text{mm}$ and $\varphi = 0$. θ and d values are listed on each plot.

ST1 and ST2 waves when $\theta = 360^\circ$. They match the extracted dispersion (contour plot) well. This demonstrates that the velocity of the ST2 wave is independent of θ for fixed d . Wang and Fehler [23] found that when $\theta = 360^\circ$, the ST2 velocity depends significantly on the total thickness of fluid in the annulus, but it is not sensitive to the radial position or even the distribution of fluid in the case where multiple layers are present. From this, we conclude that ST2 velocity does not provide information about the radial position of the fluid channel. For the CO₂ case, the ST2 is much less visible like for the water case and the velocity of ST2 cannot be used as the indicator for fluid thickness identification.

3.2 First-arrival amplitude

Here we test the sensitivity of first-arrival amplitude to θ and φ . The trough and peak of the first arrival at different receiver offsets, source frequencies, and angular positions are investigated. The CBL tool has an offset of 1m and the modernized array monopole sonic logging tool has larger offsets (more than 3m). Although other offsets are also used for tools, such as 0.6m for conventional segmented bond tool [22], we only use two offsets, 1 and 3m, to investigate the results for different receiver offsets.

First arrival with source frequency

First, we give two examples of the sensitivity of trough and peak of first-arrival amplitude at 1 m offset for different source frequencies. Fig. 9 shows an example for $\theta = 30^\circ$. Fig. 10 shows an example for $\theta = 210^\circ$. Parameters r and d are fixed at 122mm and 8mm. $\varphi = 0^\circ$. The source frequencies are labeled in kHz on each curve.

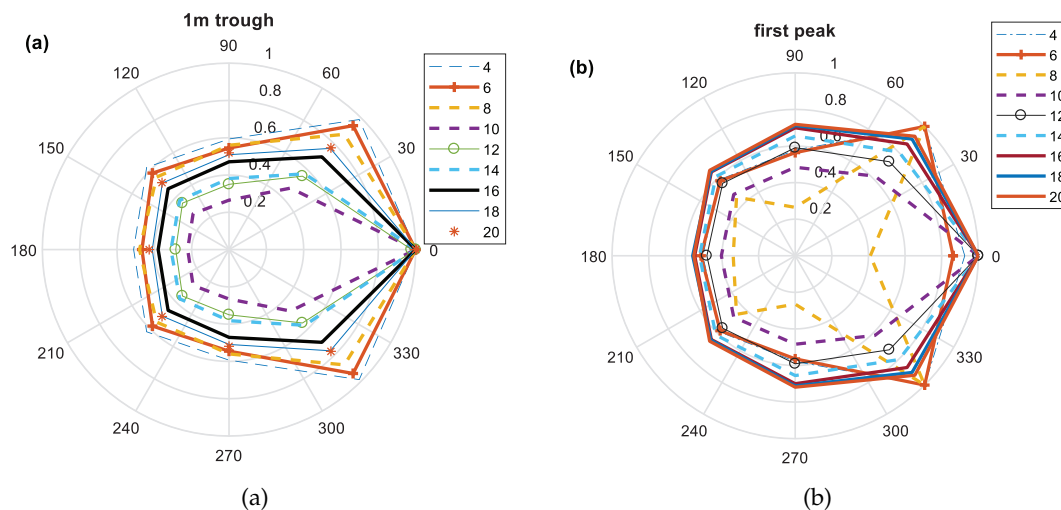
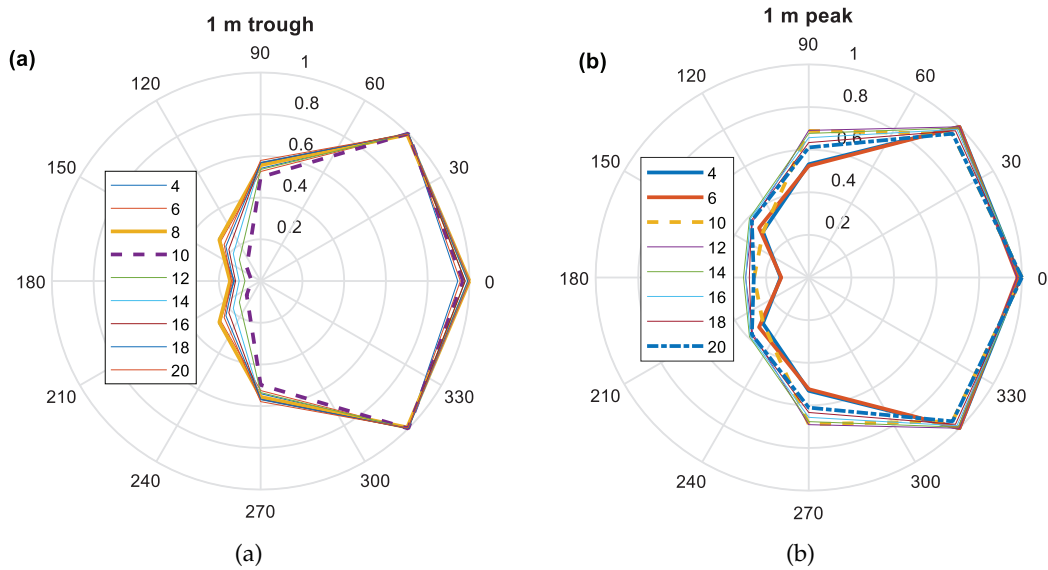


Figure 9: 9 Azimuthal variation of first-arrival amplitude for a fluid channel ($r = 122\text{mm}$, $d = 8\text{mm}$, $\theta = 30^\circ$ and $\varphi = 0^\circ$). Azimuthal axis is receiver azimuth. Radial axis is amplitude normalized by the maximum at each frequency. Source frequencies are color coded and labeled in kHz.

Figure 10: Same as Fig. 9 except for $\theta = 210^\circ$.

From these two examples, we know that azimuth angle φ of the fluid channel can be determined by the azimuthal position of the maxima for all frequencies. The amplitude at 10kHz is the most sensitive to φ . The trough is more sensitive to φ than the peak. However, because the peak has amplitude of more than 100 times that of the trough due to the polarity of our Ricker source, it is more practical to use the peak than the trough. For the other case, we plot the polarities at different source frequencies for a model ($r = 122\text{mm}$, $d = 16\text{mm}$, $\theta = 30^\circ$, and $\varphi = 0^\circ$) in Fig. 11. The polarities are the same as in Fig. 9. This further demonstrates that 10kHz is the most sensitive source frequency to φ . The frequency that is most sensitive to φ may depend on borehole dimensions, but we did not study that.

Comparing Figs. 9 and 10, we infer that the azimuthal variation of amplitude becomes less sensitive to the azimuthal position of the fracture when θ is larger. We further illustrated this in Fig. 12, which shows the distribution of the normalized first peak with receiver azimuth for fluid channels with different θ ($r = 122\text{mm}$, $d = 8\text{mm}$, and $\varphi = 0^\circ$). It is clear that the amplitude depends on both channel φ and θ and also the receiver azimuth. Although the result for larger θ shows less azimuthal variation of amplitude, the channel φ can be determined from the position of the maximum amplitude.

First arrival with receiver location

Here we further investigate the influence of receiver position on the amplitude of the first arrival for fractures of various azimuthal extents.

Fig. 13 shows the first peak amplitude of waveforms at receivers placed the center and at 9 azimuths around the borehole for different fluid channel azimuthal extents. Receiver

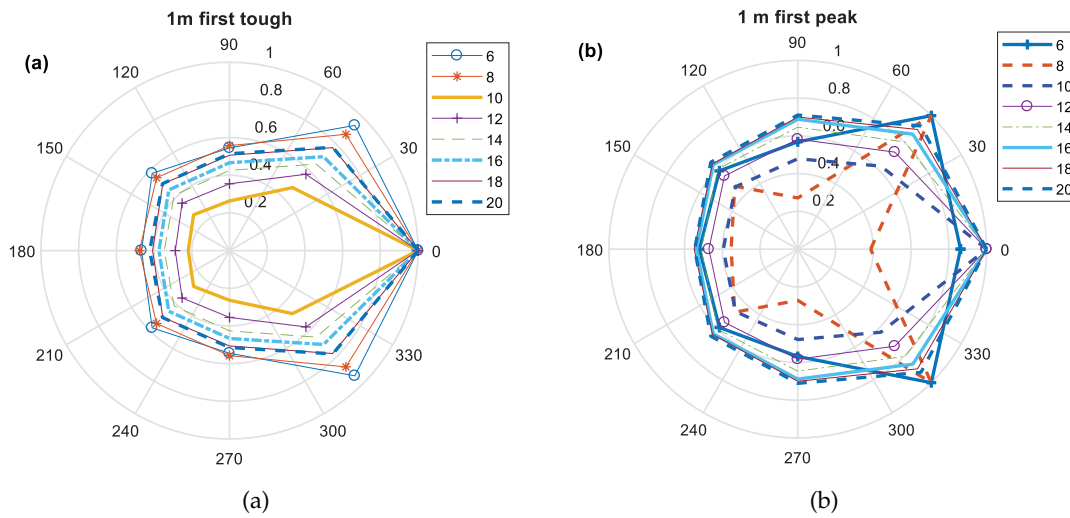


Figure 11: Same as Fig. 9 except for $d=16\text{mm}$.

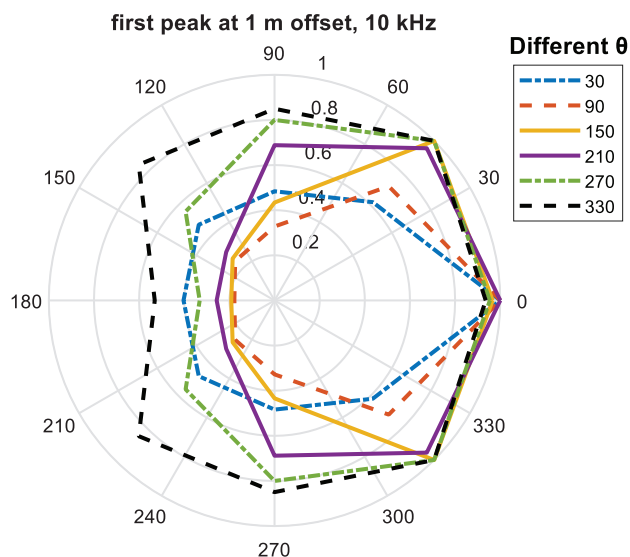


Figure 12: First-arrival amplitude distribution vs. receiver azimuth for fluid channels with different θ ($r=122\text{mm}$, $d=8\text{mm}$, and $\varphi=0^\circ$). Source frequency is 10kHz. Azimuthal axis is receiver azimuth. Radial axis is amplitude normalized by the maximum for each θ . The fluid-coverage angle θ is labeled in degrees for each curve.

offset is 1m. The source frequency is 10kHz. The amplitudes are clearly a function of receiver azimuth and θ of the fluid channel. The centralized receiver, labeled “recc”, has the largest range. The receiver at 180° has the smallest range because the receiver is the farthest one from the fluid channel so the waveform is less influenced by the channel.

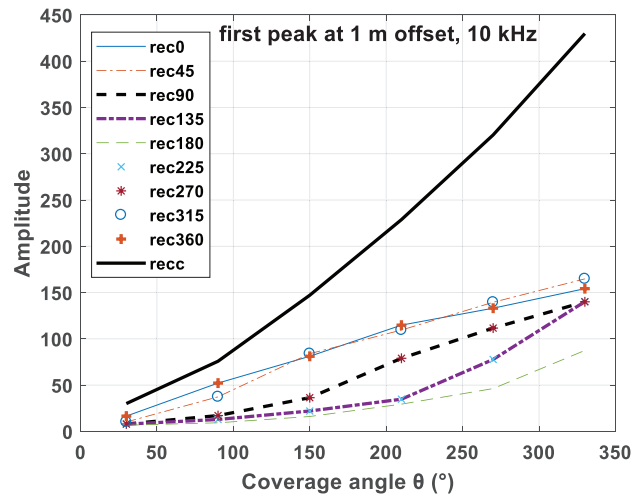


Figure 13: Peak amplitude of first arrivals at 1-m offset receivers in different locations as a function of fluid channel θ . Curves are labeled to indicate receiver location. The numbers following letter “rec” are receiver azimuth angles in degrees. “rec” is the centralized receiver. Fluid channel parameters are $r=122\text{mm}$, $d=8\text{mm}$, and $\varphi=0^\circ$. Source frequency is 10kHz.

First arrival with receiver offset

We investigate the influence of receiver offset on the amplitude ranges for different fluid channel θ when other channel parameters are fixed. Fig. 14 shows an example of normalized amplitude as a function of fluid channel θ . Four curves show results for the amplitude of peaks and troughs for two receiver offsets. The peak at 1m has the least

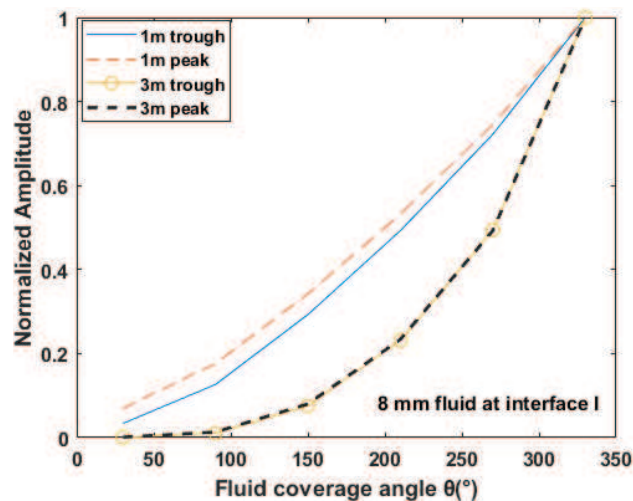


Figure 14: Normalized amplitude of peaks and troughs near the first arrival at centralized receivers with different offsets as a function of fluid channel θ . Curves are labeled to indicate the offset and which trough or peak was measured. Fluid channel parameters are $r=122\text{mm}$, $d=8\text{mm}$, and $\varphi=0^\circ$. Source frequency is 10kHz.

variation among all cases although its sensitivity is close to that of the first trough. The receiver at 3m offset has the largest-amplitude variation with channel θ . The peak and trough at 3m offset have the same variations. This implies that the casing-wave amplitude at a larger offset receiver is more sensitive to channel θ . However, for the small- θ case, such as $0 < \theta < 100^\circ$ shown in Fig. 14, the large offset receiver may lose sensitivity. In this case, a smaller offset receiver has better performance.

4 Impact

Our results show that the leak paths in cement may be assessed using different types of information obtained from centralized and azimuthally distributed receivers at different offsets. Current evaluation methods can lead to misinterpretation of the cement-to-casing bond. Various measured waveform amplitudes and arrival times of different modes can be combined and interpreted to diagnose the cement condition, including radial and azimuthal location of a fluid channel at the casing-cement boundary. The sensitivities of measurements to receiver location, offset, and source frequency that we have identified will benefit the development of a new tool. For data from existing tools, we can improve the workflow proposed in [23] to more accurately assess cement condition and leak-channel parameters. To summarize our results and provide a methodology for assessing potential fluid channels, we provide a workflow in Fig. 15, which combines the amplitude and arrival time of the first arrival at receivers at different azimuths along with ST2 velocity information. The workflow shows how one can obtain accurate measurements of d , and φ , and rough estimates of θ and r . Further improvement could be obtained by conducting an additional series of studies for $r = 170\text{mm} - d$, where $d < 48\text{mm}$. The limitation of using the first arrival at azimuth receivers is that the amplitude is not easy to pick due to the weak signal. Reliable picking requires a low-noise sensor. If the fluid channel is filled by CO_2 , the amplitude of first arrival is larger, as shown in Fig. 5. The identification is thus easier compared to the water case. The late dispersive arrival (ST2) can only be picked by experienced experts who are very familiar with wave modes. One solution is picking the modes by experts and training the picking by some machine learning method. The ST2 wave in the CO_2 case is not as clear as in the water case because of the small velocity of the super-critical CO_2 .

5 Conclusions

Current state-of-the-art cement-bond logging technology provides limited details about many leak channels associated with borehole cement. For various receiver geometries, we can use multi-modal, multi-frequency, full-waveform information to detect and characterize certain kinds of leak channels. Such characterization may be very useful for CCS management, as well as plug-and-abandonment. The details are as follows.

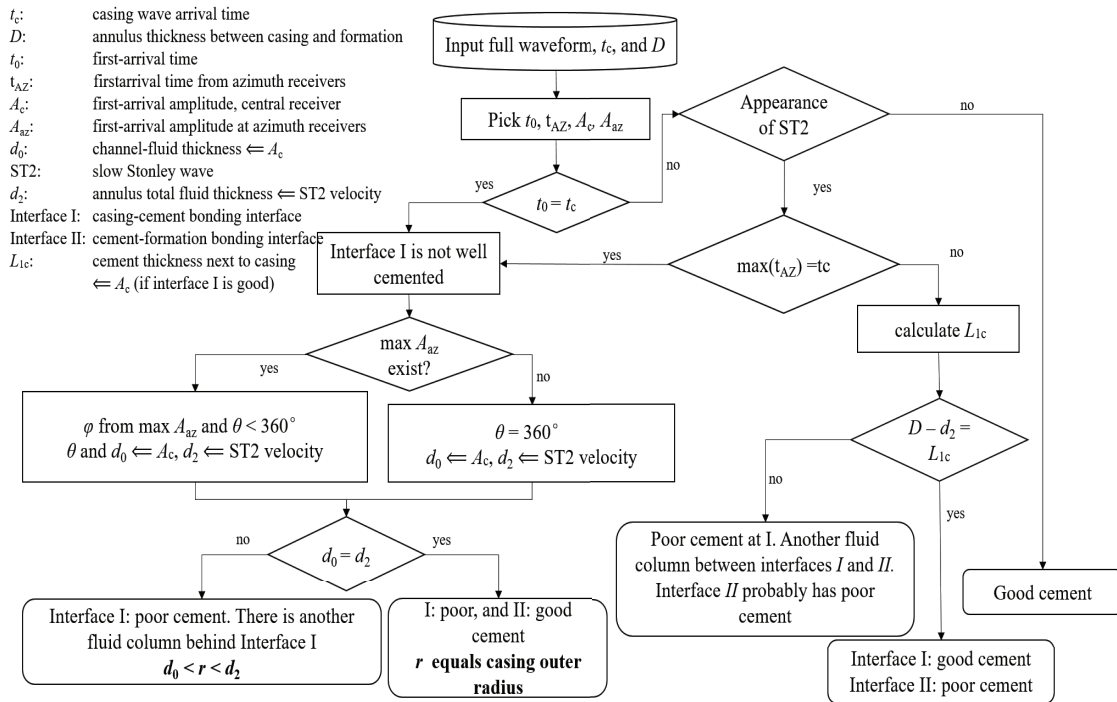


Figure 15: Workflow to assess cement condition and leak-channel parameters.

1. A channel in the borehole cement may allow CO₂ to escape. Risk assessment and remediation decisions depend on channel parameters: radial distance r ; thickness d ; azimuth φ ; coverage θ .
2. There is sensitivity to d , φ , θ of different wave modes, source frequencies, polarities, and receiver locations and offsets.
3. For the monopole measurement, the first-arrival amplitude is sensitive to θ . Amplitudes at receivers at different azimuths are sensitive to φ . The ST2 velocity is only sensitive to d . However, ST2 may not be easily picked when θ and d are small. Unfortunately, the ST2 would not be used for channel thickness identification when the channel is filled with CO₂.

Acknowledgments

This study was supported by the Founding Members Consortium of the Earth Resources Laboratory of the Massachusetts Institute of Technology (MIT) and the MIT Energy Initiative Seed Fund Award No. 015728-00149. We thank two anonymous reviewers whose comments substantially improved the presentation of our work.

References

- [1] Litynski, J., T. Rodosta, B. Brown. Best practices for monitoring, verification, and accounting of CO₂ stored in deep geologic formations - 2012 Update. US DoE, 2012.
- [2] Lumley D., 2010, 4D seismic monitoring of CO₂ sequestration. *The Leading Edge*, 2, 150-155.
- [3] Deremble L., S Loizzo M., Huet B., Lecampion, B., Quesada D., 2011, Stability of a leakage pathway in a cemented annulus. *Energy Procedia*, 4, 5283-5290.
- [4] Haldorsen J., Stensrud E., Merciu I., Miller D., 2016a, Decomposing full-waveform borehole acoustic data with application to data from a North Sea well. *Geophysics*, 81(4), IM71-IM95.
- [5] Haldorsen J., Stensrud E., Merciu I., Miller D., 2016b, Characterizing borehole plumbing using full-waveform ultrasonic data: Application to data from a North Sea well. *Geophysics*, 81(6), B189-B199.
- [6] Wang, H., Fehler M., and Miller, D., 2016a, The wavefield of acoustic logging in multiple casing models. SPWLA 57th Annual Technical Conference. Reykjavik, Iceland, 25-29 June, 2016.
- [7] Zeroug S, S Bose, B Sinha, M Skataric, Y Liu, R D'Angelo, 2016, Sonic and ultrasonic measurement applications for cased oil wells. *Insight-Non-Destructive Testing and Condition Monitoring* 58 (8), 423-430.
- [8] Gasda S. E., Bachu S., Celia M.A., 2004, Spatial characterization of the location of potentially leaky wells penetrating a deep saline aquifer in a mature sedimentary basin. *Environmental Geology*, 46,707-720.
- [9] Duguid A., Carey J.W., and Butsch R., 2014, Well integrity assessment of a 68 year old well at a CO₂ injection project. *Energy Procedia*, 63: 5691-5706.
- [10] Duguid A., Guo B., and Nygaard R., 2017, Well integrity assessment of monitoring wells at an active CO₂-EOR flood. *Energy Procedia*, 114: 5118-5138.
- [11] Wang H., M. Fehler, and A. Fournier, 2018, Assessing CO₂ leak paths by analysis of borehole wavefield modes. MITEI Seed Fund Review and Selection Meeting.
- [12] Pardue G. H., Morris R. L., Gollwitzer L. H., Moran J. H., 1963, Cement Bond Log - A study of cement and casing variables. *J. Pet. Tech.* 5, 545-555.
- [13] Walker T., 1968, A full-wave display of acoustic signal in cased holes, *J. Pet. Tech.*, 818-824.
- [14] Eyl K.A., Kurkijian A.L., Lineman D.J., Pierce E.A. Steiner J.M., 1991, Method and apparatus for determining compressional first arrival times from waveform threshold crossing provided by apparatus disposed in a sonic well tool. US Patent No. US 5058078A, 15. Jan 1991, US 07/425,661. LINK: <http://www.google.com/patents/US4985873>.
- [15] Wang H., Tao G., Shang X., 2016b, Understanding acoustic methods for cement bond logging. *The Journal of Acoustical Society of America* 139 (5), 2407-2416.
- [16] Hayman A. J., Hutin R., Wright P. V., 1991, High-resolution cementation and corrosion imaging by ultrasound. Society of Petrophysicists and Well Log Analysts 32nd Annual Symposium.
- [17] He X., Chen H., Wang X., 2014, Ultrasonic leaky flexural waves in multilayered media: Cement bond detection for cased wellbores. *Geophysics*, 79(2), A7-A11.
- [18] Viggan E. M., Johansen T. F., Merciu I., 2016, Simulation and modeling of ultrasonic pitch-catch through-tubing logging, *Geophysics*, 81(4), D383-D393.
- [19] Schlumberger, 1989, Cased Hole Log Interpretation Principles/Applications, Forth Printing March, 1997, SMP-7025. Page 5-9.
- [20] Song R., Liu J., Lv X., Yang X., Wang K., Sun L., 2013, Effects of tool eccentricity on cement-bond-log measurements: Numerical and experimental results. *Geophysics*, 78 (4):

- D181-D191.
- [21] Che X., Qiao W., Ju X., and Wang R., 2016, Azimuthal cement evaluation with an acoustic phased-arc array transmitter: numerical simulations and field test. *Applied Geophysics*, 13(1), 194-202.
 - [22] Song R., He L., 2018, Cement bond evaluation method in horizontal wells using segmented bond tool, *Geophysical Journal International*. ggy048, <https://doi.org/10.1093/gji/ggy048>.
 - [23] Wang H. and Fehler M., 2018a, The wavefield of acoustic logging in a cased-hole with a single casing-Part I: a monopole tool. *Geophysical Journal International* 212 (1), 612-626.
 - [24] van Kuijk R., Zeroug S., Froelich B., Allouche M., Bose S., Miller D., Calvez J., Schoepf V., 2005, A novel ultrasonic cased-hole imager for enhanced cement evaluation, *International Petroleum Technology Conference*, paper 10546.
 - [25] Close D., D. Cho, F. Horn, H. Edmondson, 2009, The sound of sonic: A historical perspective and introduction to acoustic logging. *Schlumberger Oil Field Rev.*, 30, 34-43.
 - [26] Wang, H., Tao, G. M.C. Fehler, 2015, Investigation of the high-frequency wavefield of an off-center monopole acoustic logging-while-drilling tool, *Geophysics*, 80, D329-D341.
 - [27] Wang, H, Tao, G, Shang, X, Fang, X, and Burns, D., 2013, The stability of Finite Difference numerical simulations of acoustic Logging-While-Drilling with different perfectly matched layer schemes, *Applied Geophysics*, 10 (3), 384-396.
 - [28] Yam H. and Schmitt D. R., 2011, CO₂ rock physics: A laboratory study. *Recovery-2011 CSPG CSEG CWLS Convention*. 1-7.
 - [29] Wang H. and Fehler M., 2017, A cement bond logging method based on full waveform measurement. *SEG Technical Program Expanded Abstracts*, 2017, 875-879.
 - [30] Rao R, and Toksöz M.N., 2005, Dispersive wave analysis - method and applications. *Earth Resources Lab Consortium Annual report*.